Research Article | Vol. 36, No. 12 / December 2019 / Journal of the Optical Society of America A 2005

Journal of the Optical Society of America A
OPTICS, IMAGE SCIENCE, AND VISION

Coherence modification and phase singularities on scattering by a sphere: Mie formulation

Hugo F. Schouten,[1] David G. Fischer,[2] and Taco D. Visser[1,3,*]

[1]Department of Physics and Astronomy, Vrije Universiteit, Amsterdam, The Netherlands
[2]NASA Glenn Research Center, Cleveland, Ohio 44135, USA
[3]The Institute of Optics, University of Rochester, Rochester, New York 14627, USA
*Corresponding author: t.d.visser@vu.nl

Received 20 August 2019; revised 10 October 2019; accepted 21 October 2019; posted 21 October 2019 (Doc. ID 375971); published 14 November 2019

When light that is spatially partially coherent, such as sunlight, is incident on a sphere, the scattered field exhibits surprising coherence properties. The observed oscillatory behavior with deep minima means that the field in certain pairs of directions is highly correlated, whereas in others, it is essentially uncorrelated, and can even have correlation singularities. Because any subsequent scattering event is strongly affected by the state of coherence, these results are particularly important for multiple scattering in discrete disordered media.

https://doi.org/10.1364/JOSAA.36.002005

1. INTRODUCTION

The scattering of a monochromatic plane wave by a homogeneous sphere, as illustrated in Fig. 1(a), is a canonical problem in physics [1–3]. Its many applications [4] in, e.g., astronomy, climate studies, medicine, and technology, have warranted the generalization of the classical theory to objects that are non-spherical [5] or non-deterministic [6,7].

Under practical circumstances the incident light is not always spatially fully coherent. This is the case, for example, for sunlight and for light that is generated by a multi-mode laser. The same holds for light that has been scattered more than once in random or disordered media. A relatively new line of research deals with scattering of such partially coherent fields. For example, the influence of spatial coherence on the angular distribution of the scattered intensity has been examined in [8–14], and strong effects are predicted for the case when the transverse coherence length is comparable to the sphere radius.

If the incident field is partially coherent, then so is the scattered field [see Fig. 1(b)]. However, the topic of the present study, the coherence properties of fields scattered by a sphere, has until now received little attention. A notable exception is a numerical study by Marasinghe *et al.* [15], who demonstrated the existence of so-called coherence vortices, singularities of the electromagnetic spectral degree of coherence, in the vicinity of a scattering sphere. These vortices occur at pairs of points at which the field is completely uncorrelated.

In this study, we formulate an analytic model for the coherence properties of partially coherent light scattered by a sphere. Of specific interest is the correlation of the far-zone field scattered in a pair of directions $\mathbf{u}_1$ and $\mathbf{u}_2$. In view of the large coherence effects on scattering that we just mentioned, this is particularly relevant for cooperative single scattering from two-dimensional structures. Examples of this are scattering in the cornea [16] and by droplets on a glass pane [17]. It is also relevant for multiple scattering in three-dimensional discrete media for which phase is preserved and coherence effects are important, including enhanced backscattering from disordered media [18–21], as well as transport in media with short- or long-range order [22–24]. Such media include discrete lattice photonic structures [25] and biomedical tissue [26]. Our results may have implications for atmospheric studies [27] because the transverse coherence length of sunlight (approximately 50 μm [28,29]) is similar in size to many atmospheric aerosols. Furthermore, spatial coherence plays a crucial role in light management in solar cells [30].

In this paper, we use scalar Mie theory to investigate the scattering of Gaussian-correlated light. We find that the spatial coherence of the scattered field displays strong oscillations: in certain pairs of directions, it can be quite large, whereas in other directions, it can be very low or even singular. Until now, correlation singularities [31–35] have been studied in the spatial domain $(\mathbf{r}_1, \mathbf{r}_2)$. Here, we report the occurence of correlation singularities of the far-zone field in the angular domain (θ_1, θ_2). While we have not considered the electromagnetic case here, we expect our results to be valid when the incident field is either unpolarized or linearly polarized.

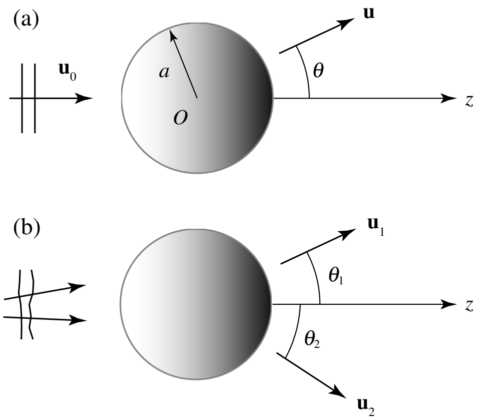

Fig. 1. Mie scattering: (a) a monochromatic plane wave travels in a direction $\mathbf{u}_0$ and is incident on a homogeneous sphere. A part of the field is scattered at an angle θ, in a direction $\mathbf{u}$. (b) If the incident field is spatially partially coherent, the field scattered in two directions $\mathbf{u}_1$ and $\mathbf{u}_2$, at angles θ_1 and θ_2 with the z axis, will be partially correlated.

2. MIE SCATTERING WITH PARTIALLY COHERENT FIELDS

Let us begin by considering a monochromatic, plane scalar wave of frequency ω and with unit amplitude, which is propagating in a direction specified by a unit vector $\mathbf{u}_0$ [see Fig. 1(a)]. We express this wave as

$$V^{(i)}(\mathbf{r}, t) = U^{(i)}(\mathbf{r}, \omega)e^{-\mathrm{i}\omega t}, \tag{1}$$

where $\mathbf{r}$ denotes a point in space and t a moment in time, and

$$U^{(i)}(\mathbf{r}, \omega) = e^{\mathrm{i}k\mathbf{u}_0\cdot\mathbf{r}}, \tag{2}$$

where $k = \omega/c$ is the wavenumber, c being the speed of light. If this field is incident on a scatterer, then the time-independent part $U(\mathbf{r}, \omega)$ of the total field that results from the scattering process may be written as the sum of the incident field $U^{(i)}(\mathbf{r}, \omega)$ and the scattered field $U^{(s)}(\mathbf{r}, \omega)$, i.e.,

$$U(\mathbf{r}, \omega) = U^{(i)}(\mathbf{r}, \omega) + U^{(s)}(\mathbf{r}, \omega). \tag{3}$$

In the far zone of the medium, the field that is scattered in the direction $\mathbf{u}$ takes the asymptotic form

$$U^{(s)}(r\mathbf{u}, \omega) \sim f(\mathbf{u}, \mathbf{u}_0, \omega)\frac{e^{\mathrm{i}kr}}{r} \quad (kr \to \infty), \tag{4}$$

where $f(\mathbf{u}, \mathbf{u}_0, \omega)$ is the scattering amplitude.

Let us next assume that the incident field is not a plane wave, but is of a more general form. Its time-independent part $U^{(i)}(\mathbf{r}, \omega)$ can then be written as an angular spectrum (Section 3.2 36), i.e., as a superposition of plane wave modes, each propagating along a direction specified by a unit vector $\mathbf{u}'$ that points into the halfspace $z > 0$, viz.,

$$U^{(i)}(\mathbf{r}, \omega) = \int_{|\mathbf{u}'_\perp|^2\leq 1} a(\mathbf{u}'_\perp, \omega)e^{\mathrm{i}k\mathbf{u}'\cdot\mathbf{r}}\mathrm{d}^2u'_\perp. \tag{5}$$

Here, $\mathbf{u}'_\perp = (u'_x, u'_y)$ is the two-dimensional projection of the vector $\mathbf{u}'$ onto the xy plane, and $a(\mathbf{u}'_\perp, \omega)$ denotes an amplitude. We then have that

$$U^{(s)}(r\mathbf{u}, \omega) = \frac{e^{\mathrm{i}kr}}{r}\int_{|\mathbf{u}'_\perp|^2\leq 1} a(\mathbf{u}'_\perp, \omega) f(\mathbf{u}, \mathbf{u}', \omega)\mathrm{d}^2u'_\perp. \tag{6}$$

When, in addition, the field is partially coherent, we must take into account its cross-spectral density function at a pair of points $\mathbf{r}_1 = r_1\mathbf{u}_1$ and $\mathbf{r}_2 = r_2\mathbf{u}_2$, namely (Section 4.3.2 [36]),

$$W^{(i)}(r_1\mathbf{u}_1, r_2\mathbf{u}_2, \omega) = \langle U^{(i)*}(r_1\mathbf{u}_1, \omega)U^{(i)}(r_2\mathbf{u}_2, \omega)\rangle, \tag{7}$$

where the angular brackets represent the average over an ensemble of field realizations. On substituting from Eq. (5) into Eq. (7), we obtain the expression

$$W^{(i)}(r_1\mathbf{u}_1, r_2\mathbf{u}_2) = \int_{|\mathbf{u}'_\perp|^2\leq 1}\int_{|\mathbf{u}''_\perp|^2\leq 1} \mathcal{A}(\mathbf{u}'_\perp, \mathbf{u}''_\perp) \times e^{\mathrm{i}k(\mathbf{u}''_\perp\cdot\mathbf{r}_2 - \mathbf{u}'_\perp\cdot\mathbf{r}_1)}\mathrm{d}^2u'_\perp\mathrm{d}^2u''_\perp, \tag{8}$$

where

$$\mathcal{A}(\mathbf{u}'_\perp, \mathbf{u}''_\perp) = \langle a^*(\mathbf{u}'_\perp)a(\mathbf{u}''_\perp)\rangle \tag{9}$$

is the angular correlation function of the incident field (Section 5.6.3 [36]) and where, for brevity, we have omited the ω dependence of the various quantities. In a similar fashion, we find for the cross-spectral density of the scattered field the formula

$$W^{(s)}(r_1\mathbf{u}_1, r_2\mathbf{u}_2) = \langle U^{(s)*}(r_1\mathbf{u}_1)U^{(s)}(r_2\mathbf{u}_2)\rangle, \tag{10}$$

$$= \frac{e^{\mathrm{i}k(r_2-r_1)}}{r_1r_2}\int_{|\mathbf{u}'_\perp|^2\leq 1}\int_{|\mathbf{u}''_\perp|^2\leq 1} \mathcal{A}(\mathbf{u}'_\perp, \mathbf{u}''_\perp) \times f^*(\mathbf{u}_1, \mathbf{u}') f(\mathbf{u}_2, \mathbf{u}'')\mathrm{d}^2u'_\perp\mathrm{d}^2u''_\perp. \tag{11}$$

The spectral degree of coherence, the normalized version of this correlation function, is defined as

$$\mu^{(s)}(r_1\mathbf{u}_1, r_2\mathbf{u}_2) \equiv \frac{W^{(s)}(r_1\mathbf{u}_1, r_2\mathbf{u}_2)}{[S^{(s)}(r_1\mathbf{u}_1)S^{(s)}(r_2\mathbf{u}_2)]^{1/2}}, \tag{12}$$

where the spectral density is given by the cross-spectral density function evaluated at two coincident points, i.e.,

$$S^{(s)}(r\mathbf{u}) = W^{(s)}(r\mathbf{u}, r\mathbf{u}). \tag{13}$$

According to scalar Mie theory {Eq. (4.66) [37]}, the scattering amplitude for a dielectric sphere with radius a and refractive index n is given by the expression

$$f(\mathbf{u}, \mathbf{u}_0) = \frac{1}{k}\sum_{l=0}^{\infty}(2l+1)\exp(\mathrm{i}\delta_l)\sin\delta_l P_l(\mathbf{u}\cdot\mathbf{u}_0), \tag{14}$$

where $\mathbf{u}\cdot\mathbf{u}_0 = \cos\theta$, with θ the scattering angle, P_l is the Legendre polynomial of order l, and the phase shifts $\delta_l(\omega)$ are {Eqs. (4.113b) and (4.153) [37]}

$$\tan\delta_l = \frac{kn\, j_l(ka)\, j'_l(kna) - k\, j_l(kna)\, j'_l(ka)}{kn\, j'_l(kna)\, n_l(ka) - k\, j_l(kna)\, n'_l(ka)}. \tag{15}$$

Here, j_l denotes the spherical Bessel function of order l, and n_l the spherical Neumann function of order l.

We will apply Eqs. (12) and (13) to the important class of so-called *Gaussian-correlated fields* with an amplitude A_0 that is assumed to be constant across an area that is larger than the sphere size (Section 5.6.4 [36]). The cross-spectral density function of such fields in the plane $z = 0$, which is taken to pass through the center O of the sphere (see Fig. 1), equals

$$W^{(i)}(\boldsymbol{\rho}_1, \boldsymbol{\rho}_2) = A_0^2 \exp[-(\boldsymbol{\rho}_2 - \boldsymbol{\rho}_1)^2/2\sigma^2]. \quad \textbf{(16)}$$

In this formula, $\boldsymbol{\rho} = (x, y)$ denotes a two-dimensional position vector of a point in the plane $z = 0$, and the transverse coherence length σ is independent of position, but may depend on frequency. The angular correlation function of the incident field is related to its cross-spectral density by the expression {Eq. (5.6)–(49) [36]}

$$\mathcal{A}(\mathbf{u}'_\perp, \mathbf{u}''_\perp) = k^4\, \tilde{W}^{(i)}(-k\mathbf{u}'_\perp, k\mathbf{u}''_\perp), \quad \textbf{(17)}$$

with the four-dimensional spatial Fourier transform defined as

$$\tilde{W}^{(i)}(\mathbf{f}_1, \mathbf{f}_2) = \frac{1}{(2\pi)^4} \int_{-\infty}^{\infty} \int_{-\infty}^{\infty} W^{(i)}(\boldsymbol{\rho}_1, \boldsymbol{\rho}_2) \cdot e^{-\mathrm{i}(\mathbf{f}_1\cdot\boldsymbol{\rho}_1 + \mathbf{f}_2\cdot\boldsymbol{\rho}_2)} \mathrm{d}^2\rho_1 \mathrm{d}^2\rho_2. \quad \textbf{(18)}$$

A calculation of the Fourier transform of Eq. (16) gives us

$$\tilde{W}^{(i)}(-k\mathbf{u}'_\perp, k\mathbf{u}''_\perp) = \frac{A_0^2\sigma^2}{2\pi} \delta^2[k(\mathbf{u}''_\perp - \mathbf{u}'_\perp)] \times \exp\left[-\frac{\sigma^2 k^2(\mathbf{u}'_\perp + \mathbf{u}''_\perp)^2}{8}\right]. \quad \textbf{(19)}$$

On substituting from Eqs. (17) and (19) into Eq. (11), we find for the cross-spectral density of the scattered field the formula

$$W^{(s)}(r_1\mathbf{u}_1, r_2\mathbf{u}_2) = \frac{e^{\mathrm{i}k(r_2 - r_1)}}{r_1 r_2} \frac{A_0^2 k^2 \sigma^2}{2\pi} \int_{|\mathbf{u}'_\perp|^2 \le 1} e^{-k^2\sigma^2 u'^2_\perp/2} \times f^*(\mathbf{u}_1, \mathbf{u}')\mathbf{f}(\mathbf{u}_2, \mathbf{u}')\mathrm{d}^2\mathbf{u}'_\perp, \quad \textbf{(20)}$$

with the scattering amplitude f given by Eq. (14). A numerical evaluation of this equation yields both the spectral density and the spectral degree of coherence of the scattered Mie field in the far zone.

3. RADIANT INTENSITY OF THE SCATTERED FIELD

The radiant intensity of the scattered field is defined by

$$I(\mathbf{u}) = r^2 S^{(s)}(r\mathbf{u}), \quad (kr \to \infty). \quad \textbf{(21)}$$

A typical example of its angular distribution is shown in Fig. 2, where the sphere radius a is taken to be 10λ, with λ the free-space wavelength. As noted in Refs. [9,10], the deep intensity minima that occur in the spatially coherent case are strongly reduced when the transverse coherence length is comparable to the size of the scatter. Here, as in the following examples, we take the refractive index to be that of water droplets, i.e., $n = 1.33$.

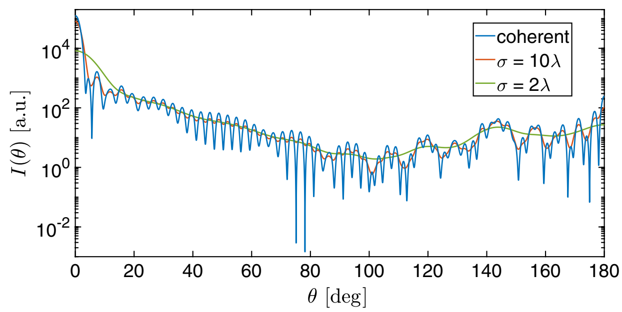

Fig. 2. Angular distribution of the radiant intensity of the scattered field for (a) fully coherent plane wave (blue curve); (b), (c) Gaussian-correlated field with transverse coherence length $\sigma = 10\lambda$ (red) and 2λ (green), respectively. Notice that the vertical axis is logarithmic. In these examples, the refractive index $n = 1.33$, and the sphere radius a is taken to be 10λ.

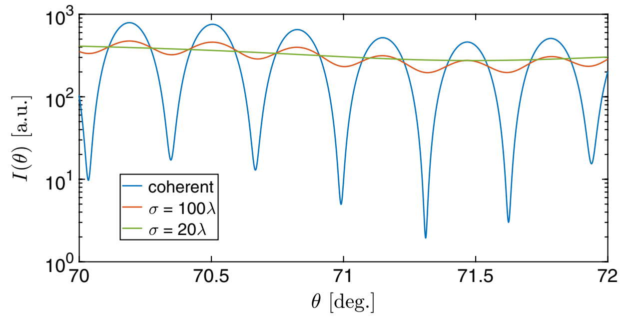

Fig. 3. Radiant intensity of the scattered field for (a) fully coherent plane wave (blue curve); (b), (c) Gaussian-correlated field with transverse coherence length $\sigma = 100\lambda$ (red) and 20λ (green), respectively. The vertical axis is logarithmic, and the horizontal axis is restricted to the interval $70° \le \theta \le 72°$. In these examples, the refractive index $n = 1.33$, and the sphere radius $a = 100\lambda$.

When the size of the scatterer increases, the angular oscillations of the scattered intensity become more rapid. This is expected because for larger spheres, the accrued path difference between waves varies quicker than for small spheres. This effect is illustrated for a representative angular interval in Fig. 3, where the particle radius is chosen as $a = 100\lambda$. Just as for the smaller sphere shown in Fig. 2, the minima are strongly reduced as the coherence length σ decreases.

In any scattering process, two directions are of specific interest, namely, the forward ($\theta = 0°$) and the backward direction ($\theta = 180°$). The former is related to the transmittance of a particulate medium, and the latter to its reflectance. In single scattering, both directions display a maximum of intensity that, as seen in Fig. 2, can be orders of magnitude larger than the field scattered in other directions. These maxima are both drastically reduced when the incident field becomes spatially partially coherent. For the forward direction, which is associated with the Poisson spot (Section 10.3.4 [38]), this is illustrated in Fig. 4. For small values of the coherence length, the intensity $I(\theta = 0°)$ scales with σ^2, in agreement with Eq. (20). The radiant intensity saturates when the coherence length is greater than the sphere radius a.

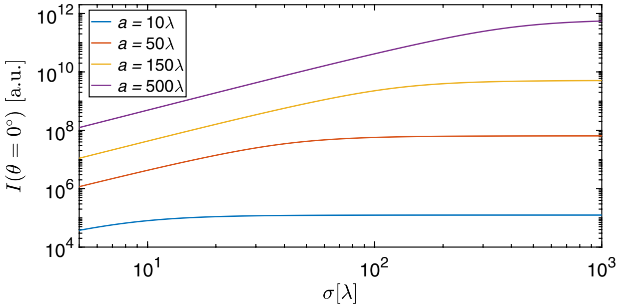

Fig. 4. Radiant intensity of the forward-scattered field, $I(\theta = 0^\circ)$, as a function of the transverse coherence length σ, expressed in wavelengths, for spheres with different radii. Blue curve: sphere radius $a = 10\lambda$; red curve: $a = 50\lambda$; orange curve: $a = 150\lambda$; purple curve: $a = 500\lambda$. In these examples, the refractive index $n = 1.33$. Note that both axes are on a logarithmic scale.

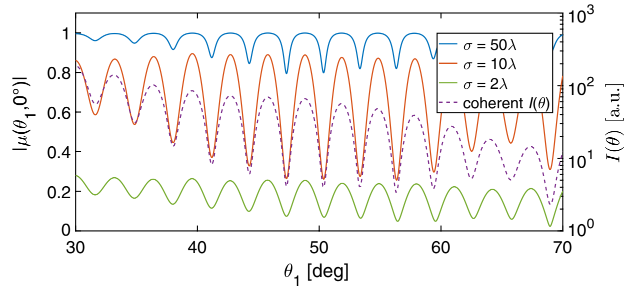

Fig. 6. Absolute value of $\mu(\theta_1, 0^\circ)$: the spectral degree of coherence between the field scattered in a direction θ_1 and the forward scattered field ($\theta = 0^\circ$). The transverse coherence length $\sigma = 50\lambda$ (blue curve), 10λ (red curve), and 2λ (green curve). For comparison, the spectral density is also plotted (dashed purple curve). In all examples, $n = 1.33$ and $a = 10\lambda$. Notice that the horizontal axis is limited to the interval $30^\circ \le \theta_1 \le 70^\circ$.

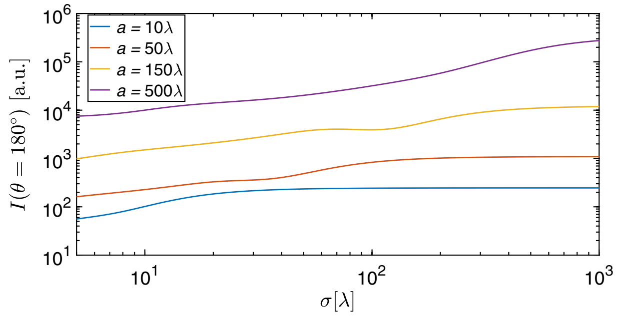

Fig. 5. Radiant intensity of the back-scattered field, $I(\theta = 180^\circ)$, as a function of the transverse coherence length σ for spheres with different radii. Blue curve: sphere radius $a = 10\lambda$; red curve: $a = 50\lambda$; orange curve: $a = 150\lambda$; purple curve: $a = 500\lambda$. In these examples, the refractive index $n = 1.33$.

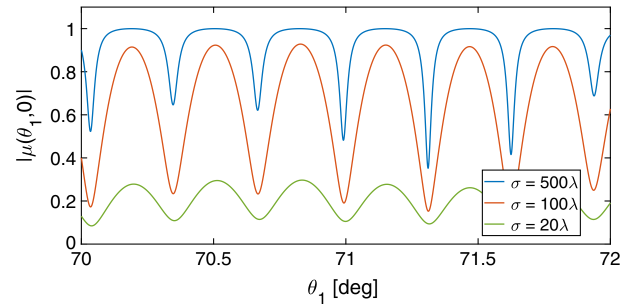

Fig. 7. Absolute value of $\mu(\theta_1, 0^\circ)$: the spectral degree of coherence between the field scattered in a direction θ_1 and the forward scattered field. In this example, the particle radius $a = 100\lambda$, and $n = 1.33$. Notice that the horizontal axis is limited to the interval $70^\circ \le \theta_1 \le 72^\circ$.

A similar dependence on the coherence length is shown by the radiant intensity of the backscattered field, $I(\theta = 180^\circ)$. This can be seen in Fig. 5, where the same sphere sizes as in Fig. 4 are examined. Large spheres are again seen to display a larger variation in the scattered intensity than smaller spheres. We next turn our attention to the state of coherence of the far-zone scattered field.

4. COHERENCE PROPERTIES OF THE SCATTERED FIELD

A first illustration of the behavior of the spectral degree of coherence, $\mu(\theta_1, \theta_2)$, is presented in Fig. 6, where the correlation of the field scattered in the direction θ_1 with the forward-scattered field ($\theta_2 = 0^\circ$) is plotted for a representative interval. We note that the angular coherence displays an oscillatory behavior similar to the radiant intensity. It is interesting to compare this correlation with the minimum value of the spectral degree of coherence of the field that is incident on the sphere, denoted by $\mu^{(i)}_{\min}$. According to Eq. (16), this occurs when the separation between the two positions $\boldsymbol{\rho}_1$ and $\boldsymbol{\rho}_2$ reaches its maximum, i.e., when $(\boldsymbol{\rho}_1 - \boldsymbol{\rho}_2)^2 = 4a^2$. For the three curves plotted in Fig. 6, we thus find that $\mu^{(i)}_{\min} = 0.92$, 0.14, and 2×10^{-22}, respectively. For the almost fully coherent case (i.e., the upper, blue curve), $|\mu(\theta_1, 0^\circ)|$ is typically close to unity, as expected. However, for a few angles, $|\mu(\theta_1, 0^\circ)| < \mu^{(i)}_{\min}$. This happens, for example, near $\theta_1 = 47.3^\circ$, where the modulus of μ is 0.79. For the middle (red) curve we see that the correlation is strongly oscillating. In this case, the maxima can be as high as 0.89. For the lower, green curve, even though $\mu^{(i)}_{\min}$ is only 2×10^{-22}, we see that the scattered field is partially coherent, with $|\mu(\theta_1, 0^\circ)|$ oscillating around 0.2. For all three curves, the minima are approximately located at the same location. Remarkably, these minima coincide with the angular minima of the scattered field intensity. This is evident from comparing the dashed purple curve with the three other ones. These results demonstrate that the state of coherence of the field can be either increased or decreased by Mie scattering.

This strong modification of the state of coherence also happens for larger spheres, as shown in Fig. 7 for the case $a = 100\lambda$. It is seen that the oscillations become both larger and faster. It is remarkable that even when the transverse coherence length is much larger than the sphere size (upper, blue curve), the correlation of the forward-scattered field and the field in a direction θ_1 can be quite low. Again, this happens when θ_1 is near the minima of the field intensity shown in Fig. 3. Furthermore, just as in

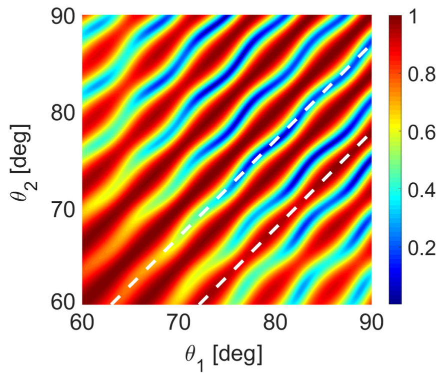

Fig. 8. Density plot of the modulus of the spectral degree of coherence between pairs of scattering angles θ_1 and θ_2. The sphere radius is taken to be $a = 5\lambda$, the refractive index $n = 1.33$, and the coherence length of the incident field $\sigma = 5\lambda$.

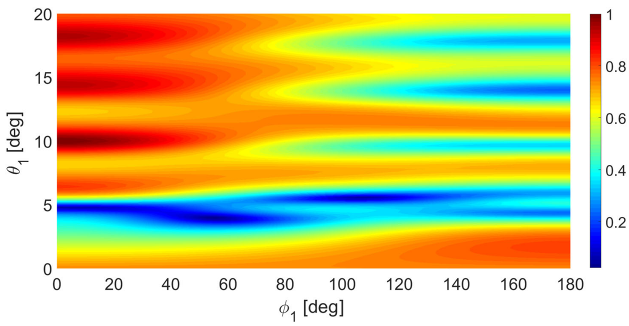

Fig. 9. Density plot of the absolute value of the spectral degree of coherence in the far field at a pair of directions, with one direction fixed at $\theta_2 = 10°$ and $\phi_2 = 0°$, and the other direction (θ_1, ϕ_1) varied. The parameters are taken as $\sigma = a = 10\lambda$ and $n = 1.33$.

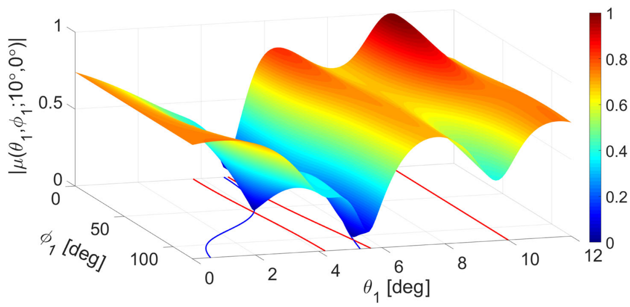

Fig. 10. Combination of two plots: above a three-dimensional, color-coded plot of $|\mu(\theta_1, \phi_1; 10°, 0°)|$, the modulus of the spectral degree of coherence of the far-zone field in a pair of directions, with one direction kept fixed at $\theta_2 = 10°$ and $\phi_2 = 0°$ and with the other direction (θ_1, ϕ_1) being varied. Below, the blue and red curves are contours of $\mathrm{Re}[\mu(\theta_1, \phi_1; 10°, 0°)] = 0$ and $\mathrm{Im}[\mu(\theta_1, \phi_1; 10°, 0°)] = 0$, respectively. At the intersection of these two curves, the spectral degree is exactly zero, indicating a coherence singularity. Note that the ϕ_1 axis is reversed to create a better viewpoint. The parameters are taken as $\sigma = a = 10\lambda$ and $n = 1.33$.

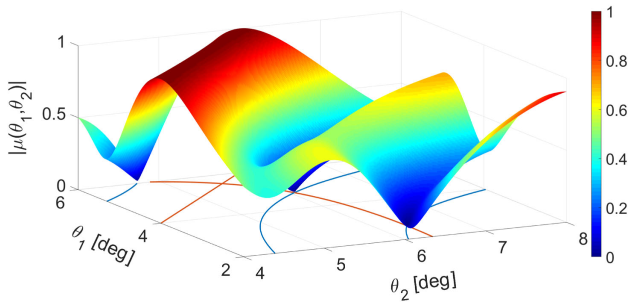

Fig. 11. Three-dimensional plot of $|\mu(\theta_1, \theta_2)|$, the modulus of the spectral degree of coherence of the field scattered in a pair of directions θ_1 and θ_2. The blue and red curves on the bottom plane are contours of $\mathrm{Re}[\mu(\theta_1, \theta_2)] = 0$ and $\mathrm{Im}[\mu(\theta_1, \theta_2)] = 0$, respectively. The intersections of these curves indicate coherence singularities. The intersection of the two red curves represents a phase saddle. In this example, $a = 10\lambda$, $n = 1.33$, and $\sigma = 10\lambda$.

Fig. 6, the minima of the three curves are approximately at the same positions. Just as with the radiant intensity, the oscillations of $|\mu(\theta_1, 0°)|$ become sharper when the transverse coherence length increases.

In Fig. 8, the two scattering angles θ_1 and θ_2 are both varied. The modulus of the spectral degree of coherence displays a more or less diagonal pattern. The two dashed white lines each correspond to pairs of nearby directions, with $\Delta\theta = \theta_2 - \theta_1 = 3.0°$ and 12.1°, respectively. Along the upper line, the correlation is relatively low, whereas along the lower line, the correlation is typically high.

Up till now, we have considered scattering angles in the same azimuthal plane ($\phi_1 = \phi_2$). The ϕ dependence of the spectral degree of coherence is shown in Fig. 9. Notice that the variation of $|\mu(\theta_1, \phi_1; \theta_2, \phi_2)|$ is considerably faster in the θ_1 direction as compared to that in the ϕ_1 direction. The deep minima (dark blue areas) contain zeros, as we will show in the next section.

5. COHERENCE SINGULARITIES

Coherence singularities are phase singularities of the correlation function. They occur at pairs of points where the field is completely uncorrelated [31–35]. Here, we investigate the occurence of a new class of objects that may be called *angular coherence singularities*, i.e., pairs of directions (rather than positions) for which $\mu(\theta_1, \phi_1; \theta_2, \phi_2) = 0$. It turns out that such topological objects occur generically in Mie scattering.

In Fig. 10, the modulus of the spectral degree of coherence $\mu(\theta_1, \phi_1; 10°, 0°)$ and the contours of the zeros of its real and imaginary parts are shown for the same parameter settings as in the previous figure. One scattering direction, (θ_2, ϕ_2), is kept fixed, whereas the other is varied in the vicinity of (θ_2, ϕ_2). It is seen that the modulus of the degree of coherence attains all values between zero and one. The value one occurs only when the two scattering directions coincide. The value zero occurs at directions where both the real and the imaginary part of the degree of coherence are zero, i.e., at the intersections of the red and blue curves. These points are so-called coherence singularities: the modulus of μ there is zero, and hence its phase is undefined. Two such singularities are visible, but there are many more outside of the plotted domain.

A second example is shown in Fig. 11. Here the two scattering directions are chosen to have the same azimuthal angle

($\phi_1 = \phi_2$). It is seen from the color-coded surface that the modulus of the spectral degree of coherence again ranges from zero to unity as θ_1 and θ_2 are varied. The two contour intersections in the bottom plane are angular coherence singularities. The intersection of two red curves represents a phase saddle where, since $\mathrm{Im}[\mu(\theta_1, \theta_2)] = 0$ there, the phase is either 0 or π.

6. CONCLUSION

We have studied Mie scattering of a partially coherent, scalar beam. The influence of the state of coherence on the forward- and backward-scattered intensity was found to be significant. Also, the correlation properties of the far-zone scattered field were seen to display a surprisingly rich behavior, with Mie-like oscillations of the spectral degree of coherence. Whereas in certain pairs of directions the coherence of the scattered field can be quite high, in other directions, it can be very low or even singular. Coherence singularities, pairs of directions that are completely uncorrelated, are found to occur generically. Because Mie scattering is highly sensitive to the state of coherence, our results are relevant for the analysis of radiation transport through systems in which multiple scattering of partially coherent fields takes place.

Funding. Air Force Office of Scientific Research (FA9550-16-1-0119).

REFERENCES

1. G. Mie, "Beiträge zur Optik trüber Medien, speziell kolloidaler Metallösungen," Ann. Phys. **25**, 377–445 (1908).
2. H. C. van de Hulst, *Light Scattering by Small Particles* (Dover, 1981).
3. M. Born and E. Wolf, *Principles of Optics*, 7th ed. (Cambridge University, 1995).
4. W. Hergert and T. Wriedt, eds., *The Mie Theory—Basics and Applications* (Springer, 2012).
5. M. I. Mishchenko, J. W. Hovenier, and L. D. Travis, eds., *Light Scattering by Nonspherical Particles* (Academic, 2000).
6. T. D. Visser, D. G. Fischer, and E. Wolf, "Scattering of light from quasi-homogeneous sources by quasi-homogeneous media," J. Opt. Soc. Am. A **23**, 1631–1638 (2006).
7. O. Korotkova, "Design of weak scattering media for controllable light scattering," Opt. Lett. **40**, 284–287 (2015).
8. D. Cabaret, S. Rossano, and C. Brouder, "Mie scattering of a partially coherent beam," Opt. Commun. **150**, 239–250 (1998).
9. T. van Dijk, D. G. Fischer, T. D. Visser, and E. Wolf, "Effects of spatial coherence on the angular distribution of radiant intensity generated by scattering on a sphere," Phys. Rev. Lett. **104**, 173902 (2010).
10. D. G. Fischer, T. van Dijk, T. D. Visser, and E. Wolf, "Coherence effects in Mie scattering," J. Opt. Soc. Am. A **29**, 78–84 (2012).
11. J. Liu, L. Bi, P. Yang, and G. W. Kattawar, "Scattering of partially coherent electromagnetic beams by water droplets and ice crystals," J. Quant. Spectrosc. Radiat. Transfer **134**, 74–84 (2014).
12. Y. Wang, H. F. Schouten, and T. D. Visser, "Tunable, anomalous Mie scattering using spatial coherence," Opt. Lett. **40**, 4779–4782 (2015).
13. Y. Wang, H. F. Schouten, and T. D. Visser, "Strong suppression of forward or backward Mie scattering by using spatial coherence," J. Opt. Soc. Am. A **33**, 513–518 (2016).
14. J. A. Gonzaga-Galeana and J. R. Zurita-Sanchez, "Mie scattering of partially coherent light: controlling absorption with spatial coherence," Opt. Express **26**, 2928–2943 (2018).
15. M. L. Marasinghe, M. Premaratne, and D. M. Paganin, "Coherence vortices in Mie scattering of statistically stationary partially coherent fields," Opt. Express **18**, 6628–6641 (2010).
16. R. W. Hart and R. A. Farrell, "Light scattering in the cornea," J. Opt. Soc. Am. **59**, 766–774 (1969).
17. J. A. Lock and C.-L. Chiu, "Correlated light scattering by a dense distribution of condensation droplets on a window pane," Appl. Opt. **33**, 4663–4671 (1994).
18. M. P. V. Albada and A. Lagendijk, "Observation of weak localization of light in a random medium," Phys. Rev. Lett. **55**, 2692–2695 (1985).
19. P. E. Wolf and G. Maret, "Weak localization and coherent backscattering of photons in disordered media," Phys. Rev. Lett. **55**, 2696–2699 (1985).
20. T. Okamoto and T. Asakura, "Enhanced backscattering of partially coherent light," Opt. Lett. **21**, 369–371 (1996).
21. E. Akkermans and G. Montambaux, *Mesoscopic Physics of Electrons and Photons* (Cambridge University, 2007).
22. V. Gaind, D. Lin, and K. J. Webb, "Solution of the Bethe-Salpeter equation in a nondiffusive random medium having large scatterers," J. Opt. Soc. Am. B **30**, 2199–2205 (2013).
23. S. John, G. Peng, and Y. Yang, "Optical coherence propagation and imaging in a multiple scattering medium," J. Biomed. Opt. **1**, 180–191 (1996).
24. R. Pierrat, J.-J. Greffet, R. Carminati, and R. Elaloufi, "Spatial coherence in strongly scattering media," J. Opt. Soc. Am. A **22**, 2329–2337 (2005).
25. H. E. Kondakci, A. F. Abouraddy, and B. E. A. Saleh, "Discrete Anderson speckle," Optica **2**, 201–209 (2015).
26. Y. L. Kim, Y. Liu, R. K. Wali, H. K. Roy, and V. Backman, "Lowcoherent backscattering spectroscopy for tissue characterization," Appl. Opt. **44**, 366–377 (2005).
27. K. Stamnes, G. E. Thomas, and J. J. Stamnes, *Radiative Transfer in the Atmosphere and Ocean*, 2nd ed. (Cambridge University, 2017).
28. G. S. Agarwal, G. Gbur, and E. Wolf, "Coherence properties of sunlight," Opt. Lett. **29**, 459–461 (2004).
29. H. Mashaal, A. Goldstein, D. Feuermann, and J. M. Gordon, "First direct measurement of the spatial coherence of sunlight," Opt. Lett. **37**, 3516–3518 (2012).
30. S. Divitt and L. Novotny, "Spatial coherence of sunlight and its implications for light management in photovoltaics," Optica **2**, 95–103 (2015).
31. H. F. Schouten, G. Gbur, T. D. Visser, and E. Wolf, "Phase singularities of the coherence functions in Young's interference pattern," Opt. Lett. **28**, 968–970 (2003).
32. G. Gbur and T. D. Visser, "Coherence vortices in partially coherent beams," Opt. Commun. **222**, 117–125 (2003).
33. S. B. Raghunathan, H. F. Schouten, and T. D. Visser, "Correlation singularities in partially coherent electromagnetic beams," Opt. Lett. **37**, 4179–4181 (2012).
34. S. B. Raghunathan, H. F. Schouten, and T. D. Visser, "Topological reactions of correlation functions in partially coherent electromagnetic beams," J. Opt. Soc. Am. A **30**, 582–588 (2013).
35. G. J. Gbur, *Singular Optics* (CRC Press, 2017).
36. L. Mandel and E. Wolf, *Optical Coherence and Quantum Optics* (Cambridge University, 1995).
37. C. J. Joachain, *Quantum Collision Theory*, 3rd ed. (Elsevier, 1987).
38. E. Hecht, *Optics*, 5th ed. (Pearson, 2017).